

Constraining neutrino mass and extra relativistic degrees of freedom in dynamical dark energy models using Planck 2015 data in combination with low-redshift cosmological probes: basic extensions to Λ CDM cosmology

Ming-Ming Zhao¹, Yun-He Li¹, Xin Zhang^{1,2*}

¹ Department of Physics, College of Sciences, Northeastern University, Shenyang 110004, China

² Center for High Energy Physics, Peking University, Beijing 100080, China

ABSTRACT

We investigate how the properties of dark energy affect the cosmological measurements of neutrino mass and extra relativistic degrees of freedom. We limit ourselves to the most basic extensions of Λ CDM model, i.e., the w CDM model with one additional parameter w , and the w_0w_a CDM model with two additional parameters, w_0 and w_a . In the cosmological fits, we employ the 2015 CMB temperature and polarization data from the Planck mission, in combination with low-redshift measurements such as the baryon acoustic oscillations (BAO), type Ia supernovae (SN) and the Hubble constant (H_0). Given effects of massive neutrinos on large-scale structure, we further include weak lensing (WL), redshift space distortion (RSD), Sunyaev-Zeldovich cluster counts (SZ), and Planck lensing data. We find that w is anti-correlated with $\sum m_\nu$, and dynamical dark energy models allow for larger neutrino masses than Λ CDM model. Moreover, observations from large-scale structure also allow higher neutrino masses. Under the constraints from Planck+BAO+SN+ H_0 +WL+RSD+SZ+lensing, we obtain $\sum m_\nu < 0.22$ eV (95% CL) for Λ CDM, $\sum m_\nu < 0.36$ eV (95% CL) for w CDM, and $\sum m_\nu < 0.52$ eV (95% CL) for w_0w_a CDM. For the case of dark radiation, we find that w is in slight positive-correlation with N_{eff} . Under the constraints from the same data combination, we obtain $N_{\text{eff}} = 3.11 \pm 0.17$ (68% CL) for Λ CDM, $N_{\text{eff}} = 2.97^{+0.18}_{-0.19}$ (68% CL) for w CDM, and $N_{\text{eff}} = 2.95 \pm 0.19$ (68% CL) for w_0w_a CDM.

Key words: neutrino mass, extra relativistic degrees of freedom, dark radiation, dark energy, Planck CMB observation.

1 INTRODUCTION

Since the phenomenon of neutrino oscillation was revealed by the solar and atmospheric neutrino experiments, the fact that neutrinos have masses and there is a significant mixing between different neutrino species has been convincingly confirmed. However, it is a great challenge for particle physics experiments to directly measure the absolute neutrino mass scale. In fact, the neutrino oscillation experiments are only sensitive to the squared mass differences between the neutrino mass eigenstates. The current data from the solar and atmospheric neutrino experiments give $\Delta m_{21}^2 \simeq 7.6 \times 10^{-5}$ eV² and $|\Delta m_{32}^2| \simeq 2.4 \times 10^{-3}$ eV² (Olive et al. 2014), respectively. These measurements give rise to two possible mass orders, i.e., the normal hierarchy with $m_1 < m_2 \ll m_3$ and the inverted hierarchy with $m_3 \ll m_1 < m_2$.

To work out the absolute masses of neutrinos, one needs at least an additional relationship between the three neutrino mass

eigenstates. The neutrino oscillation measurements can only provide a lower limit for the sum of the neutrino masses, $\sum m_\nu \gtrsim 0.06$ eV. Actually, particle physics experiments can also measure the total mass of neutrinos, but these experiments are fairly difficult. For example, the tritium beta-decay experiments, i.e., Troitsk and Mainz, gave an upper bound, $m_\beta < 2.3$ eV (95% confidence level), where m_β is a mass to which the beta-decay experiments are sensitive (Kraus et al. 2005; Otten & Weinheimer 2008). The KATRIN (KARlsruhe TRItium Neutrino) experiment aims to measure m_β with a sensitivity of ~ 0.2 eV, which would give an upper bound for the total mass, $\sum m_\nu < 0.6$ eV (KATRIN collaboration 2001; Wolf & KATRIN Collaboration 2010). In addition, the neutrinoless double beta decay ($0\nu\beta\beta$) experiments would also measure the effective mass of Majorana neutrinos at the level of $\mathcal{O}(0.1 - 1)$ eV depending on the mixing matrix (Klapdor-Kleingrothaus et al. 2001, 2004). However, compared to the particle physics experiments, it has been found that the cosmological observations are actually more prone to be capable of measuring the absolute neutrino mass (Lesgourgues et al. 2006; Valle

* Electronic address: zhangxin@mail.neu.edu.cn

2006; Hannestad 2010; Lesgourgues et al. 2012). Massive neutrinos could leave distinct signatures on the cosmic microwave background (CMB) and large-scale structure (LSS) at different epochs of the universe's evolution (Abazajian et al. 2014). To a large extent, these signatures could be extracted from the available cosmological observations, from which the total neutrino mass could be constrained. Currently, the CMB power spectrum, combined with LSS and cosmic distance measurements, can provide tight limits on the total mass of neutrinos (Ade et al. 2013, 2015a).

The CMB temperature and polarization power spectrum from Planck 2015 in combination with the baryon acoustic oscillations (BAO) data give a 95% limit of $\sum m_\nu < 0.17$ eV based on the Λ CDM model (Ade et al. 2015a). This constraint depends much on the effect of massive neutrinos on the CMB power spectrum and BAO measurements at low redshifts. At low redshifts, neutrinos are non-relativistic, and they contribute to the expansion rate through matter density, and thus change the angular diameter distance D_A . Further, the acoustic peak scale of CMB power spectrum and distance D_V of hybrid quantity $r_s(z_{\text{drag}})/D_V$ measured by BAO are altered by the changed D_A . Besides, massive neutrinos can also affect the CMB power spectrum through the Integrated Sachs-Wolfe (ISW) effect (Hall & Challinor 2012; Lesgourgues et al. 2012; Hou et al. 2014). Increasing neutrino mass leads to the decay of gravitational potential inside the Hubble radius. As photons go through this decaying potential on their way toward observer, new anisotropies are generated by the late ISW effect. Moreover, at the period when neutrinos transform from relativistic to non-relativistic regime, they also lead the gravitational potential to decay and the new anisotropies are generated by the early ISW effect (Kaplinghat et al. 2003; Lesgourgues et al. 2006).

Massive neutrinos can also leave key signatures in the spectrum of matter fluctuations by the absence of neutrinos perturbations in matter power spectrum, and hence in some large-scale observations (Bond et al. 1980; Lesgourgues et al. 2006). For example, the weak gravitational lensing provides a potentially powerful measurement of the amplitude of matter spectrum at low redshifts with cosmic shear. The matter fluctuation spectrum is also related to the growth factor $D(z)$. The redshift space distortion (RSD) can offer a direct measurement for growth rate, $f(z)$, at several low redshifts, where $f(z) = d \ln D / d \ln a$. Recently, the cluster abundance extracted from the Planck Sunyaev-Zeldovich (SZ) catalogue is considered, which depends on measurements for the amplitude of the density perturbations today, characterized by the equivalent linear theory extrapolation, the root-mean-square mass fluctuation, σ_8 . Since massive neutrinos suppress the lensing power, the CMB lensing is also helpful for constraining the neutrino mass.

On the other hand, the cosmological measurements also allow testing the properties of the extra relativistic degrees of freedom, parameterized via N_{eff} and coined dark radiation. In the standard model, we have $N_{\text{eff}} = 3.046$ (Mangano et al. 2005). A variation in N_{eff} can also affect the CMB power spectrum through a few ways, for example, changing the redshift of the matter-radiation equality, impacting on the amplitude of the peaks at high multipoles, and the early ISW effect. Therefore, N_{eff} can be constrained by the CMB power spectrum (Bashinsky & Seljak 2004; Smith et al. 2011; Archidiacono et al. 2013). In the last few years, there have been some mild preference for a non-standard value of the extra relativistic degrees of freedom from the CMB anisotropy measurements (Komatsu et al. 2011; Dunkley et al. 2011; Keisler et al. 2011; Hinshaw et al. 2013; Hou et al. 2014). However, the recent high-precision CMB temperature spectrum from Planck leads to an evidence for a standard value of N_{eff} (Ade et al. 2015a).

The effective number of relativistic species in the universe is not clear yet, which also needs the inclusion of other astronomical direct measurements to have a cosmological probe for it. In cosmology, the total relativistic energy density in neutrinos and any other dark radiation is given in terms of the photon density ρ_γ by $\rho = N_{\text{eff}}(7/8)(4/11)^{4/3}\rho_\gamma$.

Usually, the cosmological constraints on $\sum m_\nu$ and N_{eff} are derived, based on the standard Λ CDM cosmology. In much more complicated models, using the CMB power spectrum is possible to accommodate different neutrino mass or dark radiation (Hannestad 2005; Zhang et al. 2015; Zhang 2016a). In this paper, we will consider the basic extensions of the Λ CDM model, i.e., the w CDM and w_0w_a CDM models (Chevallier & Polarski 2001; Linder 2006, 2008), in which we wish to provide the simplest examples that how the dark energy property affects the very stringent cosmological neutrino mass bound. Exploration of the effects of the dark energy property on the neutrino mass bound is based on the fact that dark energy can have effects on the CMB power spectrum through changing the acoustic peak scale, the late ISW effect, and so on (Ade et al. 2015b), while the effects can be also caused by massive neutrinos. It is well-known that the constraints on the neutrino mass will be sensitive to the dark energy property when the CMB power spectrum are utilized to have a cosmological measurement for them. To see clearly how the cosmological measurements of neutrino mass is affected by the dark energy property, we will focus on the constraints on the neutrino mass in the w CDM and w_0w_a CDM models from the CMB power spectrum. For our previous studies on this aspect, see Zhang (2016a); Wang et al. (2016b). But the cases of dark radiation in the dynamical dark energy models are not addressed in these previous works. As a supplement, we will also concentrate upon the constraints on dark radiation in these scenarios.

In the global fitting, the addition of the dynamical dark energy will increase the degeneracies in the cosmological parameters, and thus using the CMB power spectrum alone is not enough. We need to combine some geometric observations, for example, the BAO data, the type Ia supernova (SN) data, and the independent measurement of Hubble constant (H_0). Here, BAO, SN, and H_0 can break the degeneracies at the low redshifts, and they can provide strong exploration to the equation of state (EoS) of dark energy at $z \lesssim 1$. Here, to constrain the neutrino mass well, we will also use the large-scale structure observations, including the WL, RSD, SZ, and CMB lensing data.

Our motivation is clear, i.e., we wish to discuss how the property of dark energy affects the cosmological constraints on the neutrino mass and dark radiation in the basic extensions of Λ CDM. The paper is organized as follows. In Sec. 2, we describe the observations we use in this paper. In Sec. 3, we present the constraint results of the neutrinos mass in the Λ CDM, w CDM, and w_0w_a CDM models. In Sec. 4, we also present the constraints on dark radiation in the models mentioned above. Finally, we give an overall discussion in Sec. 5.

2 METHODOLOGY AND DATA

In our analysis, we allow for the inclusion of $\sum m_\nu$ or N_{eff} in the Λ CDM, w CDM, and w_0w_a CDM models. The cosmological parameters in the base Λ CDM model are

$$\{\Omega_b h^2, \Omega_c h^2, 100\theta_{\text{MC}}, \tau, n_s, \log[10^{10} A_s]\}, \quad (1)$$

where $\Omega_b h^2$ is baryon energy density, $\Omega_c h^2$ is the cold dark matter energy density, $100\theta_{\text{MC}}$ is 100 times the ratio between the sound horizon and the angular diameter distance at the decoupling, τ is the reionization optical depth, and n_s and A_s are the primordial spectral index and the amplitude of the primordial spectrum, respectively. There are extra parameters in the cosmological global fittings when considering massive neutrinos or dark radiation in the w CDM and $w_0 w_a$ CDM models. The extra cosmological parameters include $\sum m_\nu$, N_{eff} , w , w_0 , and w_a , in our analysis. We constrain the above cosmological parameters with three data combinations.

Firstly, our baseline combination is comprised of CMB measurements and BAO data. The CMB measurements include the full Planck 2015 release of TT temperature spectrum and TE and EE polarization spectrum at whole multipoles ($2 < \ell < 2900$) (Aghanim et al. 2015), and we refer to this combination as ‘‘Planck’’ in our work. We use the baryon acoustic oscillations data in good agreement with the Planck data, including the measurements from the 6dFGS ($z_{\text{eff}} = 0.1$) (Beutler et al. 2011), SDSS-MGS ($z_{\text{eff}} = 0.15$) (Ross et al. 2014), LOWZ ($z_{\text{eff}} = 0.32$) and the CMASS ($z_{\text{eff}} = 0.57$) samples of BOSS (Anderson et al. 2015). This combination is usually denoted as ‘‘Planck+BAO’’.

Secondly, to further constrain the properties of dark energy, we consider geometric measurements at low redshifts, including the type Ia supernova observation and the direct measurement of the Hubble constant. For the type Ia supernova observation, we employ the ‘‘Joint Light-curve Analysis’’ (JLA) sample (Betoule et al. 2014), compiled from the SNLS, SDSS, and the samples of several low-redshift SNe. For the local measurement of the Hubble constant, we employ the result of Efstathiou (2014), derived from a re-analysis of the Cepheid data Riess et al. (2011), with the measurement value $H_0 = 70.6 \pm 3.3 \text{ km s}^{-1} \text{ Mpc}^{-1}$. We denote the above data as SN and H_0 in the data combinations.

Thirdly, we also consider measurements from the growth of structure to constrain the neutrino mass, including weak lensing, redshift space distortions, Sunyaev-Zeldovich cluster counts, and CMB lensing. For the weak lensing data, we use the cosmic shear data provided by the CFHTLenS survey (Heymans et al. 2012; Erben et al. 2013), which perform tomographic analysis with cosmological cuts, specifically removing the angular scales $\theta < 3'$ for two lowest bin combination, angular scales $\theta < 30'$ for ξ^- for four lowest bins, and $\theta < 16'$ for two highest bins for ξ^+ . We denote this measurement as WL. The redshift space distortion data provide powerful constraints on the growth rate of structure by measuring the parameter combination $f\sigma_8(z)$. Here we follow the results of Samushia et al. (2014), employing the covariance matrix for the three parameters, D_v/r_{drag} , F_{AP} , and $f\sigma_8$. It should be noticed that one data point is repeated used for BAO at $z = 0.57$. Therefore, we exclude the BOSS-CMASS result from BAO when using two measurements simultaneously. Then, for the Sunyaev-Zeldovich cluster counts, we use the full mission data from Planck with a larger catalogue of SZ clusters (Ade et al. 2015c), which still keeps the overall mass bias characterized by $1 - b$ parameter, varied in a prior with [0.1, 1.3] range. We describe this measurement as SZ. Finally, for CMB lensing, we use the Planck lensing measurement (Ade et al. 2015b).

Our constraints are based on the latest version of the Monte Carlo Markov Chain package `CosmoMC` (Lewis et al. 2002) and we perform the method χ^2 statistic in the calculations.

3 CONSTRAINTS ON NEUTRINO MASS

In this section, we investigate the constraints on the total neutrino mass $\sum m_\nu$ in dynamical dark energy models. As mentioned above, for dynamical dark energy models, we only consider the basic extensions to Λ CDM, i.e., the w CDM model and the $w_0 w_a$ CDM model. We use three data combinations to do the analysis, which are Planck+BAO, Planck+BSH, and Planck+BSH+LSS. Here, for convenience, we use ‘‘BSH’’ to denote the joint BAO+SN+ H_0 data and use ‘‘LSS’’ to denote the joint WL+RSD+SZ+lensing data. In the following, we will first present the effects of massive neutrinos and dark energy on the observations, in particular the CMB observation, and then use the actual observations to constrain these parameters.

3.1 Effects of massive neutrinos and dynamical dark energy on CMB temperature spectrum

The CMB observation could provide an accurate measurement of the angular diameter distance D_A to last-scattering surface with the redshift $z_* \simeq 1100$, which is rather important for constraining cosmological parameters because a precise high-redshift measurement could play an significant role in determining the whole expansion history. The angular diameter distance D_A is linked to the expansion history of the universe through the relation

$$D_A(z) = \frac{1}{1+z} \int_0^z \frac{dz'}{H(z')}. \quad (2)$$

We first discuss the effects of dynamical dark energy on the CMB observation. For simplicity, we consider w CDM as an example, i.e., we assume w is a constant. Increasing w at fixed matter density increases $H(z)$ at $z \lesssim 1$ and reduces the angular-diameter distance $D_A(z)$ for $0 < z \leq z_*$ (Howlett et al. 2012). The observable $\theta_* = r_s/D_A$, θ_* determines the acoustic peak scale of CMB power spectrum, and as a consequence, the reduced $D_A(z)$ increases the peak of the CMB spectrum.

Another main effect of dark energy on CMB power spectrum is from the late ISW effect. Before the dark energy domination, the gravitational potential in the universe keeps as a constant to the first order in linear perturbation theory. When dark energy starts to dominate the universe’s evolution, the gravitational potential is not a constant any more, due to the accelerated expansion of the universe. Dark energy leads to the decay of gravitational potential on large scales, generating new anisotropies of the CMB photons. As the photons go through these decaying potentials on their way toward the observer, new anisotropies are generated by the ISW effect. Eventually, the small-scale CMB anisotropy spectrum is actually also altered.

The left panel of Fig. 1 shows how C_ℓ^{TT} changes with different EoS of dark energy w . Here, as examples, we choose three values of w , namely, $w = -0.8, -1.0$, and -1.2 , and fix $\sum m_\nu$ to be 0.06 eV and other parameters consistent with Planck (Ade et al. 2015a). The figure shows that, at the low multipoles ($2 < \ell < 50$), a smaller w leads to a suppression of temperature spectrum, i.e., a smaller C_ℓ^{TT} , due to the late ISW effect.

Massive neutrinos can also affect the CMB power spectrum, through altering expansion rate and gravitational potential (Hu & Dodelson 2002; Ichikawa et al. 2005). Initially, neutrinos are massless and behave as radiation. After recombination, massless neutrinos generally transform to massive neutrinos. In this period, neutrinos are non-relativistic, but they still contribute to energy density. However, this behavior is neglected in the Poisson equation.

As a consequence, the gravitational potential decays through the increased $H(z)$. As photons free stream immediately after decoupling, the anisotropies are created by the early ISW effect. Thus, the neutrino mass affects the CMB power spectrum.

When neutrinos are absolutely non-relativistic, they contribute to the expansion rate through the matter density. Increasing neutrino mass leads to a reduction in $H(z)$ at $z \lesssim 1$ at fixed θ_* . The decreased $H(z)$ results in a decay of gravitational potential at small scales, and thus contributes to a suppression of CMB power spectrum through the late ISW effect (Hou et al. 2014). In addition to that, the decreased $H(z)$ increases D_A .

The right panel of Fig. 1 shows how CMB temperature spectrum changes with different neutrino mass $\sum m_\nu$. Here, for example, we choose three values of $\sum m_\nu$, namely, $\sum m_\nu = 0, 0.6$ eV and 1.2 eV, and we fix w to be -1 . We find that larger neutrino masses suppress CMB spectrum at low multipoles ($2 < \ell < 50$) due to the late ISW effect.

3.2 Massive neutrinos versus dark energy

We now focus on the constraints on the neutrino mass in the w CDM and w_0w_a CDM models from the above mentioned three data combinations. According to the constraint results, we investigate the correlation between neutrino mass and dark energy property, from which we can see how the property of dark energy impacts on the cosmological measurement of neutrino mass.

The marginalized posterior contours in the $\sum m_\nu$ - w plane for the w CDM model is shown in Fig. 2. In this figure, the three data combinations give consistent results, showing that w is anti-correlated with $\sum m_\nu$. This correlation can be explained by the compensation to the effects on the acoustic peak scale θ_* . Increasing w leads $H(z)$ to increase. However, a reduction in $\sum m_\nu$ can compensate the changed $H(z)$, and there are the same D_A according to Eq. (2) and the same θ_* . The results show that a larger neutrino mass is allowed by a phantom dark energy in w CDM. The Planck+BSH combination provides the tightest constraint on $\sum m_\nu$. Once the LSS data are added, the constraint becomes looser. This is because the current LSS observations favor lower matter perturbations (demonstrated by a lower σ_8), which obviously tends to favor a larger neutrino mass due to the free-streaming effect of massive neutrinos.

For the case of the w_0w_a CDM model, we plot in Fig. 3 the marginalized posterior contours in the w_0 - w_a plane from the Planck+BAO and Planck+BSH+LSS combinations, shown as the green and red contours, respectively. The constraints in the w_0 - w_a plane from the Planck+BSH data are also shown in Fig. 3 as samples, color coded by the value of $\sum m_\nu$. From this figure, we find that a larger $\sum m_\nu$ is favored by an early phantom dark energy, more precisely, a dynamical dark energy evolving from $w < -1$ to $w > -1$.

Next, we compare the constraint results of $\sum m_\nu$ for the Λ CDM model, the w CDM model and the w_0w_a CDM model. The detailed fitting results are given in Tables 1 and 2.

The Planck+BAO data combination gives the limits: $\sum m_\nu < 0.17$ eV (95% CL) for Λ CDM (in great agreement with the result derived by the Planck collaboration), $\sum m_\nu < 0.33$ eV (95% CL) for w CDM, and $\sum m_\nu < 0.47$ eV (95% CL) for w_0w_a CDM. For w CDM, we have $w = -1.068^{+0.103}_{-0.067}$, and for w_0w_a CDM, we have $w_0 = -0.52^{+0.34}_{-0.22}$ and $w_a = -1.73^{+0.39}_{-1.25}$. We find that, compared to Λ CDM, the upper limits of neutrino mass become larger in the w CDM and w_0w_a CDM models. In the case of dynamical dark energy, we can clearly see that a phantom energy with $w < -1$ is

more favored and a quintom energy evolving from $w < -1$ to $w > -1$ is more favored by the current observations, and thus a larger $\sum m_\nu$ is more favored in the two dynamical dark energy models compared to Λ CDM.

In the joint fits to Planck+BSH, we obtain $\sum m_\nu < 0.15$ eV for Λ CDM, $\sum m_\nu < 0.25$ eV for w CDM, and $\sum m_\nu < 0.51$ eV for w_0w_a CDM. Correspondingly, we have $w = -1.042^{+0.052}_{-0.045}$ for w CDM and we have $w_0 = -0.89^{+0.12}_{-0.14}$ and $w_a = -0.84^{+0.80}_{-0.49}$ for w_0w_a CDM. We find that, in this case, the EoS of dark energy can be constrained more tightly because of the addition of SN and H_0 data. For the Λ CDM and w CDM models, the Planck+BSH data give distinctly tighter constraints on $\sum m_\nu$ than the Planck+BAO data. For the w_0w_a CDM model, the constraint of $\sum m_\nu$ becomes a little bit looser for Planck+BSH than for Planck+BAO.

Under the Planck+BSH+LSS data, the total mass of neutrinos are constrained to $\sum m_\nu < 0.22$ eV for Λ CDM, $\sum m_\nu < 0.36$ eV for w CDM, and $\sum m_\nu < 0.52$ eV for w_0w_a CDM. Correspondingly, we have $w = -1.042^{+0.057}_{-0.047}$ for w CDM and we have $w_0 = -0.96 \pm 0.11$ and $w_a = -0.47^{+0.59}_{-0.43}$ for w_0w_a CDM. We find that, compared to the case of Planck+BSH, the addition of the LSS data only makes little improvement to the constraints on dark energy. This is because the smooth dark energy affects the growth of structure only through the expansion history and thus the measurements of matter perturbations can only provide loose constraints on the property of dark energy, especially for the case that the current measurements of growth of structure are not accurate enough. But we find that, by adding the LSS data, the constraints on $\sum m_\nu$ become looser, compared to the Planck+BSH case. As mentioned above, the current LSS observations, such as WL, RSD, and SZ, prefer a universe with low matter perturbations, compared with the Planck CMB data (Ade et al. 2015a). The tension between Planck and LSS can be greatly relieved by considering massive neutrinos in the cosmological model due to the free-streaming effect of massive neutrinos tending to suppress the matter perturbations (Battye & Moss 2014; Wyman et al. 2014; Zhang & Geng & Zhang 2014). Therefore, a larger $\sum m_\nu$ is allowed when the LSS data preferring low matter perturbations are included.

Figure 4 shows the joint, marginalized constraints on $\sum m_\nu$ and σ_8 for the Λ CDM, w CDM, and w_0w_a CDM models from the data combination of Planck+BSH+LSS. We find that, in all the three models, σ_8 is indeed anti-correlated with $\sum m_\nu$. Thus, in a cosmological model, considering massive neutrinos can lead to a low σ_8 universe, making the Planck data consistent with the observations of WL, RSD, and SZ.

3.3 Neutrino mass versus other cosmological parameters in dynamical dark energy models

Dark energy can affect neutrino mass, and certainly, it also affects other parameters because of mutual compensation effect in the global fits. To compare the cases of Λ CDM, w CDM, and w_0w_a CDM, we use Planck+BAO and Planck+BSH to make an analysis.

Figure 5 shows the constraints on the neutrinos mass and $\Omega_b h^2$, Ω_m , and H_0 for the three models. We show the constraint results by using the Planck+BAO data combination in the top panel. We find that, the constrained results are quite different for different models. As the contours in the $H_0 - \sum m_\nu$ plane show, $\sum m_\nu$ is anti-correlated with H_0 in Λ CDM. Here, this correlation in the $\sum m_\nu$ and H_0 can be explained. A larger neutrino mass increases θ_* , and a reduction in H_0 can lead to the same θ_* (a smaller H_0 corresponds to a larger D_A and hence a smaller θ_*). However, the

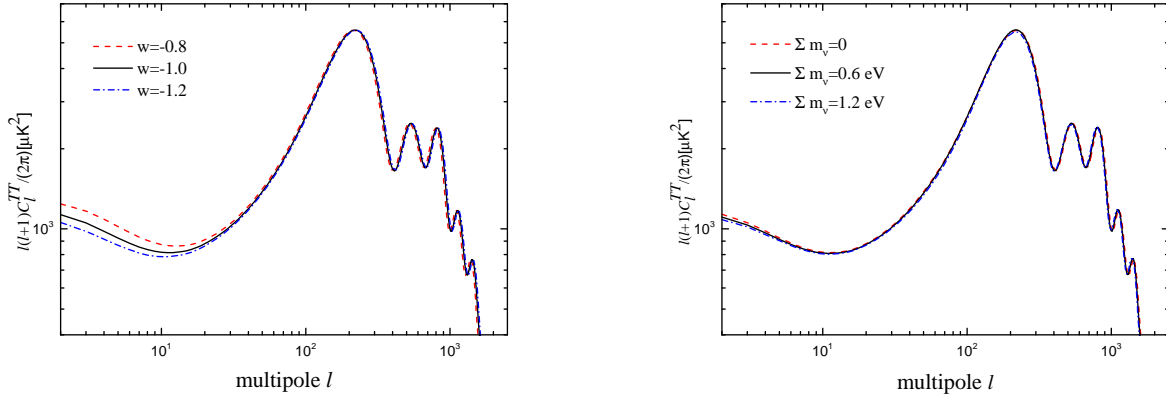


Figure 1. Left panel: The CMB temperature spectra C_ℓ^{TT} with different EoS of dark energy w . Here, we choose $w = -0.8, -1.0$ and -1.2 , and fix $\sum m_\nu$ to be 0.06 eV. At $2 < \ell < 50$, it is found that a smaller w leads to a suppression of CMB temperature power, namely, a smaller C_ℓ^{TT} , due to the late ISW effect. Right panel: the CMB temperature spectra with different total neutrino mass $\sum m_\nu$. Here, we choose $\sum m_\nu = 0, 0.6$ eV, and 1.2 eV, and fix $w = -1$. At $2 < \ell < 50$, a larger $\sum m_\nu$ leads to a smaller C_ℓ^{TT} , due to the late ISW effect.

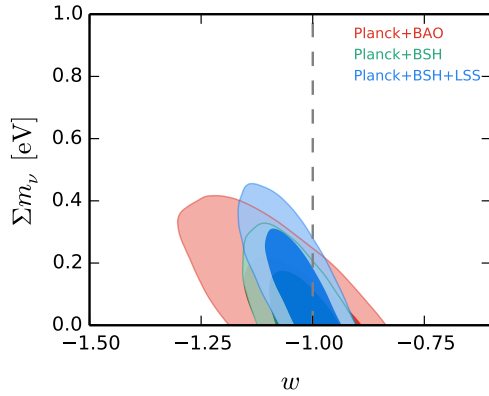


Figure 2. 68% and 95% CL contours in the $w - \sum m_\nu$ plane from the three data combinations of Planck+BAO, Planck+BSH, and Planck+BSH+LSS, where “BSH” denotes the joint of BAO, SN, and H_0 data, “LSS” denotes the combination of WL, RSD, SZ and CMB lensing data. Planck+BSH gives a tighter constraint on $\sum m_\nu$, but Planck+BSH+LSS allows a larger $\sum m_\nu$. The constraints on dark energy from the three data combinations are all compatible with Λ CDM.

correlation direction inverses in the w CDM and w_0w_a CDM models, showing a positive correlation between H_0 and $\sum m_\nu$. Planck data give a quite precise measurement on θ_* , leading to a precise constraint on $\Omega_m h^3$ in the Λ CDM model. But for the w CDM and w_0w_a CDM models, $\Omega_m h^3$ is not constrained well, with a much broader distribution (Li et al. 2013). However, the distributions of $\Omega_m h^2$ in the three models are similar. Given the comparison results of $\Omega_m h^2$ and $\Omega_m h^3$, we can find a fact that, dynamical dark energy models relax constraints on H_0 . Therefore, it is possible to exist a positive correlation between neutrino mass and H_0 . By weaker constraint on H_0 , the tension between Planck and the independent measurement of H_0 can be relieved a little by considering dynamical dark energy.

The bottom panel of Fig. 5 shows the same case with the Planck+BSH data combination. We find that when the SN and H_0 data are combined, all the constraints become tightened, in par-

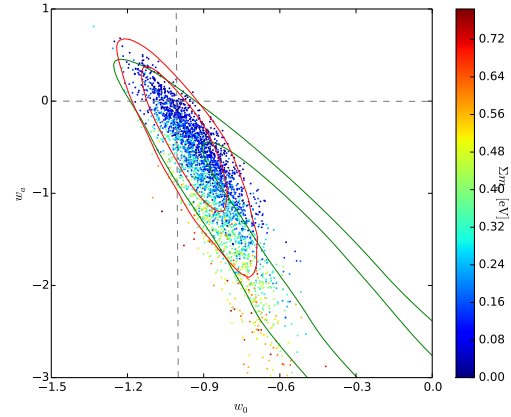


Figure 3. Samples from the Planck+BSH chains in the $w_0 - w_a$ plane, colour-coded by $\sum m_\nu$. The green contours show the constraints from the Planck+BAO data set, and the red contours show the constraints from Planck+BSH+LSS. The Λ CDM case with $w_0 = -1$ and $w_a = 0$ is shown in the plane by the cross of horizontal and vertical dashed lines. The samples show the points corresponding to larger $\sum m_\nu$ distribute the regions of w evolving from $w < -1$ to $w > -1$.

ticular for Ω_m and H_0 in the w_0w_a CDM model. As the same to the case of top panel, $\sum m_\nu$ is in anti-correlation with H_0 in the Λ CDM model, while is in slightly positive correlation with H_0 in the w CDM model and the w_0w_a CDM model. Detailed fitting results for all the parameters can be found in Tables 1 and 2.

4 CONSTRAINTS ON THE EFFECTIVE NUMBER OF RELATIVISTIC SPECIES

The relativistic energy density in the early universe include the contributions from photons and neutrinos, and possibly other extra relativistic degrees of freedom, called dark radiation. The effective number of relativistic species, including neutrinos and any other dark radiation, is defined as a parameter N_{eff} , for which the standard value is 3.046 corresponding to the case with three-generation

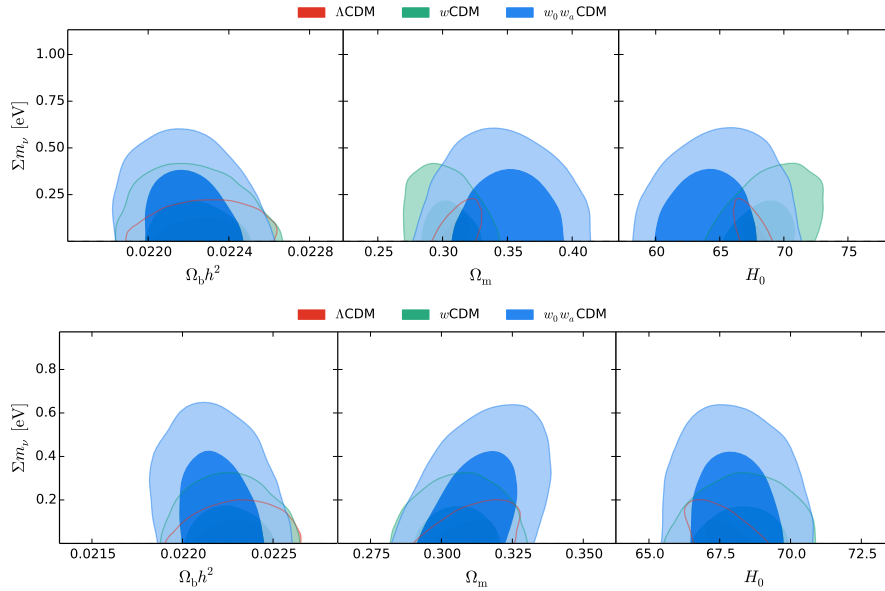


Figure 5. The 68% and 95% CL contours in the $\sum m_\nu - \Omega_b h^2$, $\sum m_\nu - \Omega_m$, $\sum m_\nu - H_0$ planes. We show the Planck+BAO constraints in the top panel and the Planck+BSH constraints in the bottom panel.

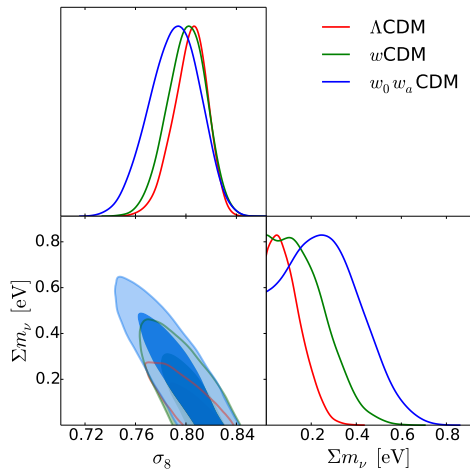


Figure 4. Joint, marginalized constraints from Planck+BSH+LSS on the Λ CDM (red), w CDM (green), and $w_0 w_a$ CDM (blue) models. The 68% and 95% CL contours in the $\sigma_8 - \sum m_\nu$ plane are shown. Note here that there is a peak in the posterior distribution of $\sum m_\nu$ for the $w_0 w_a$ CDM case around $\sum m_\nu = 0.285$ eV, but the statistical significance is rather low.

neutrinos and no extra dark radiation (Mangano et al. 2005). If the value of N_{eff} is beyond 3.046, it indicates that there is some dark radiation other than three-generation active neutrinos. The behavior of dark radiation is exactly equivalent to massless neutrinos. Thus, the total radiation energy density in the universe is given by

$$\rho_r = \rho_\gamma \left[1 + \frac{7}{8} \left(\frac{4}{11} \right)^{4/3} N_{\text{eff}} \right], \quad (3)$$

where ρ_γ is the energy density of photons. An additional ΔN_{eff} , defined by $N_{\text{eff}} - 3.046$, if found by observations, indicates the existence of dark radiation, which is important for cosmology. In

this section, we will discuss the constraints on N_{eff} in the w CDM and $w_0 w_a$ CDM models.

4.1 Effects of dark radiation on CMB temperature spectrum

Like massless neutrinos, dark radiation is treated as a free streaming fluid. They do not interact at all for $z \ll 10^{10}$. They affect the CMB power spectrum in several ways. First, varying N_{eff} shifts the redshift of matter-radiation equality, z_{eq} , defined by

$$1 + z_{\text{eq}} = \frac{\Omega_m}{\Omega_r} = \frac{\Omega_m h^2}{\Omega_r h^2} \frac{1}{1 + 0.2271 N_{\text{eff}}}. \quad (4)$$

Thus, a larger N_{eff} leads to a reduction in z_{eq} , which means the delay of radiation dominance in the universe, leading to an increase in gravitational potential and an enhancement of the early ISW effect. As a consequence, the first and second peaks of CMB power spectrum are affected.

Second, a larger N_{eff} increases the relativistic energy density and hence the expansion rate, which causes a reduction in the comoving sound horizon, r_s , through $r_s \propto 1/H$ (Archidiacono et al. 2013). If r_s is decreased, via $\theta_* = r_s/D_A$, θ_* will be decreased as well (D_A is less effected in the early universe). The reduction in θ_* leads the peak positions of the CMB power spectrum to move toward to high multipoles.

Third, a larger N_{eff} also enhances the Silk damping tail via expansion rate. The Silk damping is an effect, from the diffusion damping of oscillations in the plasma, caused by an extended decoupling process of baryon-photon interactions. The photon freely streams on scale λ_d within time distance of decoupling, and temperature fluctuation on scale smaller than this scale will be damped. The factor of damping has $\exp[-2r_d/\lambda_d]$, where r_d is diffusion length. When diffusion process approaches the last scattering, there is $r_d \propto 1/\sqrt{H}$ (Archidiacono et al. 2013), which gives the ratio of $\theta_d/\theta_s = \sqrt{H}$, where θ_d is damping angular scale. As a consequence, the increased expansion rate by increasing N_{eff} reinforces the Silk damping on small scales.

Last, a larger N_{eff} enhances the anisotropic stress at small

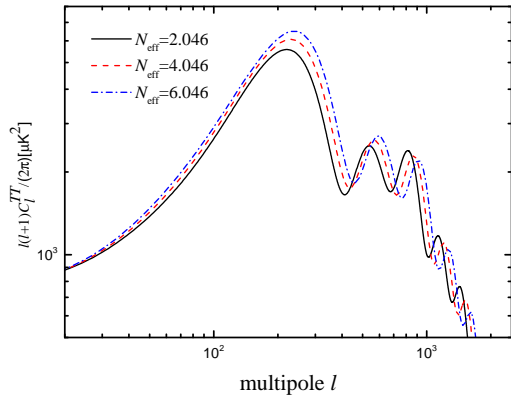


Figure 6. The CMB temperature spectra C_ℓ^{TT} with the different effective numbers of relativistic species N_{eff} . We choose $N_{\text{eff}} = 2.046, 4.046,$ and 6.046 , and fix $w = -1$ and $\sum m_\nu = 0.06$ eV. At $2 < \ell < 50$, the temperature power is mildly increased as dark radiation density increases. At $\ell \sim 200$, the amplitude of the first peak is enhanced by larger N_{eff} and peak position moves toward high multipoles due to the early ISW effect. On small scales ($\ell > 600$), a larger N_{eff} enhances the Silk damping tail of the temperature power.

scales. The distribution function of free streaming species will involve an effect from an extra anisotropic stress when N_{eff} increases, and this stress could change the gravitational potential and hence alter the degree of the reinforced small-scale anisotropy.

Figure 6 shows the C_ℓ^{TT} spectrum with different N_{eff} . We choose the three cases of N_{eff} , namely, $N_{\text{eff}} = 2.046, 4.046,$ and 6.046 , as examples, and other cosmological parameters are fixed. The figure shows that, at $\ell < 600$ multipole, a larger N_{eff} raises the CMB power spectrum. At $\ell < 50$ multipole, the power spectrum is mainly affected by the late ISW effect. Around $\ell \sim 200$ scale, the amplitude of peak is largely enhanced, and position of peak moves towards high multipole. At $\ell > 600$ scales, we can find that the Silk damping tail is clear. In our analysis, we only concentrate on the effect at large scales of $\ell < 200$, related to dark energy.

4.2 Constraints on dark radiation in dynamical dark energy models

In this section, we study the constraints on dark radiation in w CDM and $w_0 w_a$ CDM from the Planck+BAO, Planck+BSH, and Planck+BSH+LSS data combinations. Depending on the constraint results, we can probe for the correlation between w and N_{eff} , and see the effect of dark energy property on the cosmological measurement of dark radiation.

The contours in the $N_{\text{eff}}-w$ plane are shown in Fig. 7. In this figure, we can find that w is positively correlated with N_{eff} . This correlation can be explained by the compensation to the effects on the acoustic peak scale θ_* . The acoustic peak scale θ_* is determined by r_s/D_A . A larger w leads to a reduction in D_A through the increased $H(z)$. If the sound horizon is fixed, θ_* will become larger due to the decreased D_A . To keep θ_* fixed, the observable r_s has to become smaller. Here, increasing N_{eff} can lead to a smaller sound horizon r_s through the increased $H(z)$. By comparison to the constraint results of N_{eff} from the three data combinations, we find that the Planck+BSH data combination gives the largest value of N_{eff} . Once the LSS observations are included, the value of N_{eff}

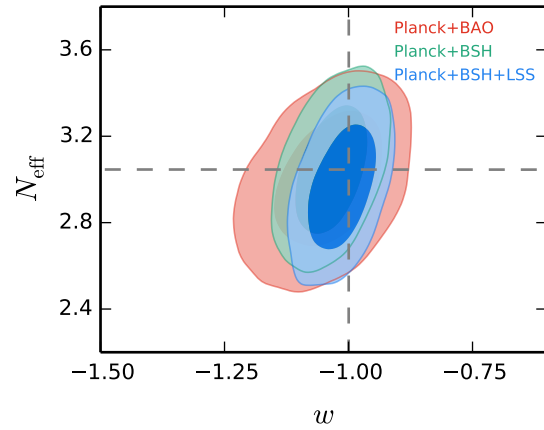


Figure 7. 68% and 95% CL contours in the $w-N_{\text{eff}}$ plane for the w CDM model. The constraints are from the three data combinations, i.e., Planck+BAO, Planck+BSH, and Planck+BSH+LSS. Note that the cross point of the grey lines show $w = -1$ and $N_{\text{eff}} = 3.046$ in the base Λ CDM. It is shown that the constraints results from the three data combination are all compatible with the base Λ CDM cosmology.

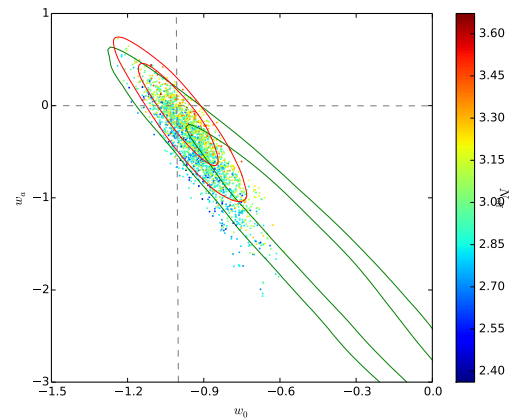


Figure 8. Samples from the Planck+BSH chains in the w_0-w_a plane, colour-coded by N_{eff} . The green contours show the constraints from the Planck+BAO data, and the red contours shows the constraints from the Planck+BSH+LSS combination. The samples show that the points corresponding to smaller N_{eff} distribute the regions of w evolving from $w < -1$ to $w > -1$.

becomes smaller. However, the constraint results of N_{eff} from the three data combinations are all compatible with the standard value of 3.046, which means that there is no evidence of deviation from the standard model of particle physics.

For the case of $w_0 w_a$ CDM model, we plot the marginalized posterior contours in the w_0-w_a plane from the Planck+BAO and Planck+BSH+LSS data combinations, and present them in Fig. 8. The samples from Planck+BSH chains in the w_0-w_a plane are also shown in Fig. 8, colour coded by the value of N_{eff} . In this figure, we can find that a smaller N_{eff} is allowed by an early phantom dark energy evolving from $w < -1$ to $w > -1$. As same as the w_0 CDM model, the $w_0 w_a$ CDM model also allows for a standard value of N_{eff} from the three data combinations.

Next, we compare the constraint results of N_{eff} for the

Λ CDM, w CDM, and w_0w_a CDM models. The fitting results are displayed in Tables 3 and 4.

The Planck+BAO data combination gives the constraints: $N_{\text{eff}} = 3.04^{+0.19}_{-0.18}$ for Λ CDM, $N_{\text{eff}} = 3.00 \pm 0.20$ for w CDM, and $N_{\text{eff}} = 2.96 \pm 0.20$ for w_0w_a CDM. Correspondingly, we have $w = -1.042^{+0.076}_{-0.065}$ for w CDM, $w_0 = -0.50^{+0.36}_{-0.25}$ and $w_a = -1.53^{+0.73}_{-1.08}$ for w_0w_a CDM. From these results, we can find that the w CDM and w_0w_a CDM models allow a smaller N_{eff} compared to Λ CDM. For the case of dynamical dark energy, we can find that the w CDM and w_0w_a CDM models are in favor of a phantom energy with $w < -1$ and a quintom energy evolving from $w < -1$ to $w > -1$, respectively. Therefore, a smaller N_{eff} is favored by the two dynamical dark energy models much better than the Λ CDM model due to the positive correlation between N_{eff} and w .

In the joint fits to Planck+BSH data, we have $N_{\text{eff}} = 3.11 \pm 0.17$ for Λ CDM, $N_{\text{eff}} = 3.05^{+0.18}_{-0.19}$ for w CDM, and $N_{\text{eff}} = 2.99^{+0.21}_{-0.19}$ for w_0w_a CDM. Correspondingly, we have $w = -1.034 \pm 0.045$ for w CDM and $w_0 = -0.92^{+0.09}_{-0.12}$ and $w_a = -0.45^{+0.49}_{-0.35}$ for w_0w_a CDM. From these results, we clearly find that the constraints on the EoS of dark energy are tighten by the inclusion of SN and H_0 data. However, by adding the SN and H_0 data, the constraints of dark radiation are looser in three models. For the Λ CDM model, the Planck+BSH data combination gives obviously looser constraint on N_{eff} than the Planck+BAO data combination. For the w CDM model and the w_0w_a CDM model, the Planck+BSH data gives slightly looser constraints on N_{eff} than the Planck+BAO data.

Further considering the LSS observations in the combination, the constraint results of dark radiation become $N_{\text{eff}} = 2.99 \pm 0.16$ for Λ CDM, $N_{\text{eff}} = 2.97^{+0.18}_{-0.19}$ for w CDM, and $N_{\text{eff}} = 2.95 \pm 0.19$ for w_0w_a CDM, respectively. For the EoS of dark energy, we have $w = -1.014 \pm 0.042$ for w CDM and $w_0 = -0.99 \pm 0.09$ and $w_a = -0.09^{+0.41}_{-0.32}$ for w_0w_a CDM. We can find that the Planck+BSH+LSS data has little contribution to the constraints on dark energy, but gives the tightest constraints on dark radiation compared to the Planck+BAO and Planck+BSH data combinations. For dark energy, as mentioned above, the LSS observations can not provide the tight constraints on w due to the effects of dark energy on the growth of structure only through the expansion history. For N_{eff} , the LSS observations prefer a lower σ_8 , which also leads to smaller values of N_{eff} due to the positive correlation between σ_8 and N_{eff} .

Figure 9 shows the constraints on N_{eff} and $\Omega_b h^2$, H_0 , and σ_8 for three models. The Planck+BAO data gives the $\Omega_b h^2 - N_{\text{eff}}$, $\sigma_8 - N_{\text{eff}}$, and $H_0 - N_{\text{eff}}$ contours in the top panel and the Planck+BSH data gives the corresponding contours in the bottom panel. From the figure, we can find that the Planck+BAO data gives the consistent constraint contours in the $\Omega_b h^2 - N_{\text{eff}}$, but a little bit different constraint contours in the $H_0 - N_{\text{eff}}$ and $\sigma_8 - N_{\text{eff}}$ planes for different models. Here, we focus on the $H_0 - N_{\text{eff}}$ plane. As the constraint contours show, the correlation between N_{eff} and H_0 is consistent in the Λ CDM, w CDM, and w_0w_a CDM models, i.e., N_{eff} is positively correlated with H_0 . This correlation can be illustrated. Planck accurately measures the acoustic scale r_s/D_A . Increasing N_{eff} leads the sound horizon at recombination to be smaller, and hence recombination has to be closer (larger H_0 and hence smaller D_A) for it to keep the same angular size observed by Planck (Ade et al. 2015a). Therefore, a larger N_{eff} favours a higher H_0 . The tension between Planck and the direct measurement of Hubble constant can be relieved by considering dark radiation in the cosmological models. However, for the constraint values of H_0 ,

the w CDM model favors a relatively larger value of H_0 , having $H_0 = 68.1 \pm 1.7 \text{ km s}^{-1} \text{ Mpc}^{-1}$, and the w_0w_a CDM model favors a lower value of H_0 , having $H_0 = 63.6^{+2.3}_{-3.2} \text{ km s}^{-1} \text{ Mpc}^{-1}$. This is because the w CDM model and the w_0w_a CDM model relax the constraints on H_0 due to the weaker constraints on dark energy under Planck+BAO, especially for the w_0w_a CDM model.

The bottom panel of Fig. 9 shows the same constraints cases from the Planck+BSH data combination. We find that once the SN and H_0 data are included, all parameter spaces are shrunk, in particular for the parameter H_0 in the w_0w_a CDM model.

5 CONCLUSION

The latest Planck data release have provided us with an extremely precise picture of the cosmic microwave background, confirming the standard Λ CDM model. However, the underlying properties of dark sector are still under discussion, such as the mass scale of neutrinos and the presence of unknown relativistic species.

Massive neutrinos and dark radiation can affect the CMB anisotropy and the matter fluctuations, thus providing a potential way to measure them through the CMB power spectra and the large-scale structure observations. However, when these observations are used to limit the neutrino mass and the extra relativistic degrees of freedom, the dark energy property would bring impacts on this cosmological constraint, due to the fact that dark energy can also affect the CMB power spectrum and the large-scale structure at late times. To find out how the property of dark energy impacts on the cosmological measurement of the neutrino mass and the extra relativistic degrees of freedom, we focus on the constraints in the basic extension of Λ CDM model, i.e., the w CDM and w_0w_a CDM models.

We select the CMB power spectrum from Planck 2015 in combination with the BAO data as baseline at the first, then add the low-redshift measurements, such as SN and H_0 direct measurement, and eventually, include the WL, RSD, SZ, and Planck lensing data. We perform comprehensive cosmological constraints on the neutrino mass and dark radiation. The Planck+BAO data gives us the constraints on the total mass of neutrinos, $\sum m_\nu < 0.17 \text{ eV}$ (95% CL) for the Λ CDM model, $\sum m_\nu < 0.33 \text{ eV}$ (95% CL) for the w CDM model, and $\sum m_\nu < 0.47 \text{ eV}$ (95% CL) for the w_0w_a CDM model. For the parameters of dark energy, we have $w = -1.068^{+0.103}_{-0.067}$ (68% CL) for the w CDM model, and $w_0 = -0.52^{+0.34}_{-0.22}$ (68% CL) and $w_a = -1.73^{+0.39}_{-1.25}$ (68% CL) for the w_0w_a CDM model. From the constraint results, we could find that the w CDM model more favors a phantom energy with $w < -1$ and the w_0w_a CDM model favors a quintom energy evolving from $w < -1$ to $w > -1$. Besides, a larger neutrino mass is favored for the two dynamical dark energy models compared to the Λ CDM model, which means that a smaller w is in favor of a larger $\sum m_\nu$. These results can be illustrated. Decreasing w can reduce the expansion rate $H(z)$ but increase the angular diameter distance D_A , which leads the acoustic peak scale θ_* to be small. To keep the same acoustic scale, one way is to increase $\sum m_\nu$. We also study the correlations in the neutrino mass and other cosmological parameters. Here, it is worth to note that there is an anti-correlation between $\sum m_\nu$ and H_0 in the Λ CDM model, but a positive correlation between $\sum m_\nu$ and H_0 in dynamical dark energy (w CDM and w_0w_a CDM) models.

The Planck+BSH data gives us the constraint results of the total mass of neutrinos, $\sum m_\nu < 0.15 \text{ eV}$ for the Λ CDM model, $\sum m_\nu < 0.25 \text{ eV}$ for the w CDM model, and $\sum m_\nu < 0.51$

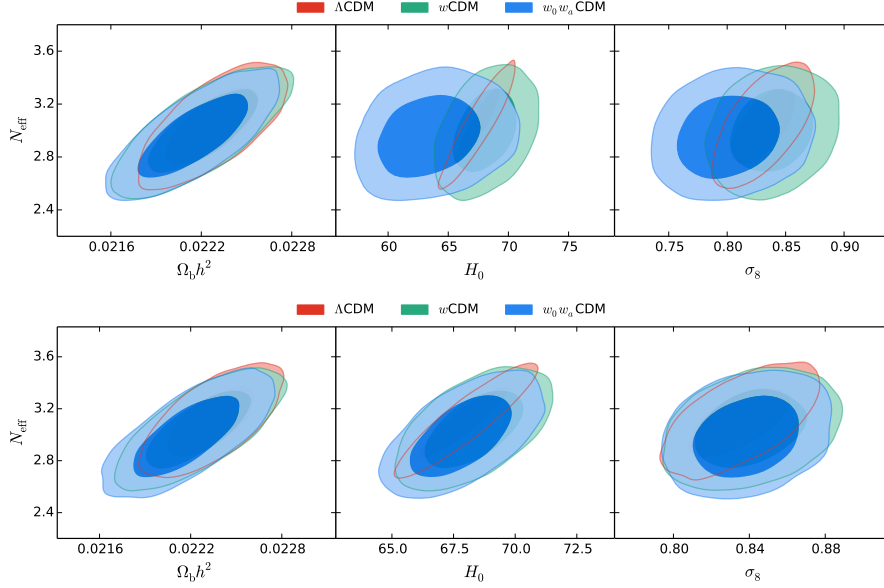


Figure 9. The 68% and 95% CL contours in the $N_{\text{eff}}-\Omega_b h^2$, $N_{\text{eff}}-H_0$, and $N_{\text{eff}}-\sigma_8$ planes. We show the Planck+BAO constraints in the top panel and the Planck+BSH constraints in the bottom panel.

eV for the $w_0 w_a$ CDM model. For the parameters of dark energy, we have $w = -1.042^{+0.057}_{-0.047}$ for the w CDM model, and we have $w_0 = -0.96 \pm 0.11$ and $w_a = -0.47^{+0.59}_{-0.43}$ for the $w_0 w_a$ CDM model. We find that the inclusion of the SN and H_0 data leads the constraints on $\sum m_\nu$ in the Λ CDM and w CDM models to be smaller compared to the Planck+BAO data. However, for the $w_0 w_a$ CDM model, the constraints on $\sum m_\nu$ is a little bit looser for the Planck+BSH data than the Planck+BAO data.

When further adding the large-scale observations to offer a more comprehensive constraint on $\sum m_\nu$, we obtain $\sum m_\nu < 0.22$ eV for the Λ CDM model, $\sum m_\nu < 0.36$ eV for the w CDM model, and $\sum m_\nu < 0.52$ eV for the $w_0 w_a$ CDM model. Correspondingly, we have $w = -1.042^{+0.057}_{-0.047}$ for the w CDM model and we have $w_0 = -0.96 \pm 0.11$ and $w_a = -0.47^{+0.59}_{-0.43}$ for the $w_0 w_a$ CDM model. From the results, we can find that the Planck+BSH+LSS data favors a larger neutrino mass compared to the Planck+BAO and Planck+BSH data. This is because massive neutrinos can suppress the matter fluctuation as free-streaming particles.

For the effective number of relativistic species, we also constrain it in the Λ CDM, w CDM, and $w_0 w_a$ CDM models using above-mentioned three data combinations. The Planck+BAO gives us the constraints: $N_{\text{eff}} = 3.14^{+0.19}_{-0.18}$ for the Λ CDM model, $N_{\text{eff}} = 3.00 \pm 0.20$ for the w CDM model, and $N_{\text{eff}} = 2.96 \pm 0.20$ for the $w_0 w_a$ CDM model. Correspondingly, we have $w = -1.042^{+0.076}_{-0.065}$ for the w CDM model and $w_0 = -0.50^{+0.36}_{-0.25}$ and $w_a = -1.53^{+0.73}_{-1.08}$ for the $w_0 w_a$ CDM model. From the constraint results, when the w CDM and $w_0 w_a$ CDM models are in favor of a phantom energy with $w < -1$ and a quintom energy evolving from $w < -1$ to $w > -1$, a smaller N_{eff} is favored for these two dynamical models compared to the Λ CDM models. Namely, a smaller w is favored for a smaller N_{eff} . Decreasing w can increase D_A through the decreased $H(z)$, which leads to the acoustic scale θ_* to be smaller. However, we can decrease N_{eff} to increase the sound horizon r_s and keep θ_* fixed. In addition, we study the correlations in dark radiation and other cosmological parameters.

Here, the positive correlation between N_{eff} and H_0 in three models is notable.

The Planck+BSH data gives us the constraint results: $N_{\text{eff}} = 3.11 \pm 0.17$ for the Λ CDM model, $N_{\text{eff}} = 3.05^{+0.18}_{-0.21}$ for the w CDM model, and $N_{\text{eff}} = 2.99^{+0.19}_{-0.21}$ for the $w_0 w_a$ CDM model. Correspondingly, we have $w = -1.034 \pm 0.045$ for w CDM and $w_0 = -0.92^{+0.09}_{-0.12}$ and $w_a = -0.45^{+0.49}_{-0.35}$ for $w_0 w_a$ CDM. From these results, we clearly find that the addition of SN and H_0 data tighten the constraints on the w of dark energy, but relax the constraints of N_{eff} in three models compared to the Planck+BAO data.

The Planck+BSH+LSS data gives the constraints: $N_{\text{eff}} = 2.99 \pm 0.16$ for Λ CDM, $N_{\text{eff}} = 2.97^{+0.18}_{-0.19}$ for w CDM, and $N_{\text{eff}} = 2.95 \pm 0.19$ for $w_0 w_a$ CDM. For the w of dark energy, we have $w = -1.014 \pm 0.042$ for w CDM and $w_0 = -0.99 \pm 0.09$ and $w_a = -0.09^{+0.41}_{-0.32}$ for $w_0 w_a$ CDM. We can find that the Planck+BSH+LSS data has little contribution to the constraints on dark energy, but gives the tightest constraints on dark radiation compared to the Planck+BAO and Planck+BSH data combinations. As a whole, the three data combinations allow for a standard value of N_{eff} in the dynamical dark energy models, i.e., 3.046, which means that there is no evidence of deviation from the standard model of particle physics.

The constraints on massive neutrinos, the effective number of relativistic species, or the the mass hierarchy, have been studied a lot in the Λ CDM model (Zhang & Li & Zhang 2014; Huang et al. 2015; Di Valentino et al. 2015, 2016), and have been more or less considered in some dynamical dark energy models in our previous works (Li & Zhang 2012; Zhang & Geng & Zhang 2014; Zhang et al. 2015; Zhang 2016a). In Zhang (2016a), we obtain a relatively lower total mass of neutrinos in the holographic dark energy model compared to other models, with $\sum m_\nu < 0.113$ eV. More attempts may help us approach the fact of neutrino physics.

Table 1. Fitting results for the Λ CDM, w CDM, and w_0w_a CDM models from the Planck+BAO and Planck+BSH data combinations, respectively. Here, we fix $N_{\text{eff}}=3.046$. We quote the $\pm 1\sigma$ errors, but for the neutrino mass $\sum m_\nu$, we quote the 95% CL upper limits. Note that $\sum m_\nu$ is in units of eV, and H_0 is in units of $\text{km s}^{-1}\text{Mpc}^{-1}$.

data Model	Planck+BAO			Planck+BSH		
	Λ CDM	w CDM	w_0w_a CDM	Λ CDM	w CDM	w_0w_a CDM
$\Omega_b h^2$	0.02228 ± 0.00015	$0.02223^{+0.00016}_{-0.00015}$	0.02220 ± 0.00015	0.02230 ± 0.00014	0.02226 ± 0.00015	0.02219 ± 0.00015
$\Omega_c h^2$	0.1192 ± 0.0011	0.1197 ± 0.0014	0.1200 ± 0.0014	0.1191 ± 0.0011	0.1195 ± 0.0013	$0.1201^{+0.0014}_{-0.0013}$
$100\theta_{\text{MC}}$	$1.04083^{+0.0003}_{-0.00031}$	$1.04075^{+0.00032}_{-0.00031}$	1.04069 ± 0.00032	1.04086 ± 0.00030	1.04078 ± 0.00031	1.04068 ± 0.00031
τ	0.082 ± 0.017	0.081 ± 0.018	$0.079^{+0.018}_{-0.017}$	0.083 ± 0.017	0.081 ± 0.017	$0.080^{+0.017}_{-0.018}$
w/w_0	...	$-1.068^{+0.103}_{-0.067}$	$-0.52^{+0.22}_{-0.34}$...	$-1.042^{+0.052}_{-0.045}$	$-0.89^{+0.12}_{-0.14}$
w_a	$-1.73^{+0.39}_{-1.25}$	$-0.84^{+0.80}_{-0.49}$
Σm_ν	< 0.17	< 0.33	< 0.47	< 0.15	< 0.25	< 0.51
n_s	0.9659 ± 0.0041	0.9645 ± 0.0046	$0.9630^{+0.0046}_{-0.0045}$	0.9664 ± 0.0041	0.9652 ± 0.0044	$0.9626^{+0.0046}_{-0.0047}$
$\ln(10^{10} A_s)$	3.097 ± 0.033	$3.096^{+0.035}_{-0.034}$	3.093 ± 0.034	3.099 ± 0.033	$3.096^{+0.033}_{-0.032}$	3.095 ± 0.034
Ω_m	$0.3128^{+0.0073}_{-0.0075}$	0.3040 ± 0.0140	$0.3490^{+0.0300}_{-0.0250}$	$0.3109^{+0.0067}_{-0.0075}$	0.3060 ± 0.0090	0.3130 ± 0.0110
H_0	$67.4^{+0.6}_{-0.5}$	$68.7^{+1.6}_{-1.9}$	$64.5^{+2.2}_{-3.1}$	$67.6^{+0.6}_{-0.5}$	68.31 ± 1.0	68.0 ± 1.1
σ_8	$0.829^{+0.019}_{-0.016}$	0.836 ± 0.023	$0.792^{+0.029}_{-0.033}$	$0.831^{+0.018}_{-0.015}$	$0.835^{+0.020}_{-0.019}$	$0.821^{+0.031}_{-0.024}$
χ^2_{min}	12940.94	12939.28	12938.46	13657.29	13653.50	13656.78

Table 2. Fitting results for the Λ CDM, w CDM, and w_0w_a CDM from the Planck+BSH+LSS data combination. Here, we fix $N_{\text{eff}}=3.046$. We quote the $\pm 1\sigma$ errors, but for the neutrino mass $\sum m_\nu$, we quote the 95% CL upper limits. Note that $\sum m_\nu$ is in units of eV, and H_0 is in units of $\text{km s}^{-1}\text{Mpc}^{-1}$.

Data Model	Planck+BSH+LSS		
	Λ CDM	w CDM	w_0w_a CDM
$\Omega_b h^2$	0.02235 ± 0.00014	0.02231 ± 0.00014	0.02227 ± 0.00015
$\Omega_c h^2$	0.1178 ± 0.0011	0.1181 ± 0.0012	0.1184 ± 0.0012
$100\theta_{\text{MC}}$	1.04096 ± 0.00030	1.04090 ± 0.00030	1.04083 ± 0.00031
τ	$0.066^{+0.014}_{-0.016}$	0.067 ± 0.015	0.068 ± 0.015
w/w_0	...	$-1.042^{+0.057}_{-0.047}$	-0.96 ± 0.11
w_a	$-0.47^{+0.59}_{-0.43}$
Σm_ν	< 0.22	< 0.36	< 0.52
n_s	$0.9684^{+0.0040}_{-0.0041}$	$0.9672^{+0.0042}_{-0.0043}$	0.9656 ± 0.0046
$\ln(10^{10} A_s)$	$3.062^{+0.027}_{-0.030}$	3.064 ± 0.029	3.065 ± 0.028
Ω_m	$0.3072^{+0.0071}_{-0.0082}$	$0.3053^{+0.0085}_{-0.0086}$	$0.3090^{+0.0100}_{-0.0101}$
H_0	$67.8^{+0.7}_{-0.6}$	68.3 ± 1.0	68.2 ± 1.0
σ_8	$0.803^{+0.015}_{-0.012}$	$0.800^{+0.017}_{-0.014}$	$0.791^{+0.022}_{-0.019}$
χ^2_{min}	13906.47	13905.66	13904.06

Table 3. Fitting results for the Λ CDM, w CDM, and w_0w_a CDM models from the Planck+BAO and Planck+BSH data combinations, respectively. Here, we fix $\sum m_\nu=0.06$ eV. We quote the $\pm 1\sigma$ errors. Note that H_0 is in units of $\text{km s}^{-1}\text{Mpc}^{-1}$.

data Model	Planck+BAO			Planck+BSH		
	Λ CDM	w CDM	w_0w_a CDM	Λ CDM	w CDM	w_0w_a CDM
$\Omega_b h^2$	0.02228 ± 0.00019	0.02221 ± 0.00023	0.02215 ± 0.00023	0.02234 ± 0.00019	$0.02225^{+0.00022}_{-0.00021}$	$0.02217^{+0.00022}_{-0.00024}$
$\Omega_c h^2$	$0.1192^{+0.0031}_{-0.0033}$	$0.1191^{+0.0030}_{-0.0031}$	0.1189 ± 0.0031	$0.1200^{+0.0029}_{-0.0030}$	0.1196 ± 0.0030	$0.1194^{+0.0031}_{-0.0030}$
$100\theta_{\text{MC}}$	$1.04085^{+0.00044}_{-0.00045}$	$1.04087^{+0.00044}_{-0.00043}$	$1.04088^{+0.00044}_{-0.00047}$	1.04076 ± 0.00042	$1.0408^{+0.00042}_{-0.00046}$	$1.04081^{+0.00045}_{-0.00044}$
τ	$0.082^{+0.016}_{-0.017}$	$0.078^{+0.019}_{-0.018}$	0.074 ± 0.018	0.084 ± 0.016	0.080 ± 0.017	$0.073^{+0.017}_{-0.016}$
w/w_0	...	$-1.042^{+0.076}_{-0.065}$	$-0.50^{+0.36}_{-0.23}$...	-1.034 ± 0.045	$-0.92^{+0.09}_{-0.11}$
w_a	$-1.53^{+0.23}_{-1.08}$	$-0.45^{+0.49}_{-0.35}$
N_{eff}	$3.04^{+0.19}_{-0.18}$	3.00 ± 0.20	2.96 ± 0.20	3.11 ± 0.17	$3.05^{+0.18}_{-0.19}$	$2.99^{+0.19}_{-0.21}$
n_s	0.9657 ± 0.0075	0.9627 ± 0.0091	0.9605 ± 0.009	0.9686 ± 0.0069	$0.965^{+0.0083}_{-0.0084}$	0.9611 ± 0.009
$\ln(10^{10} A_s)$	$3.097^{+0.035}_{-0.036}$	$3.088^{+0.040}_{-0.039}$	$3.080^{+0.037}_{-0.040}$	3.103 ± 0.034	$3.095^{+0.039}_{-0.036}$	$3.080^{+0.035}_{-0.034}$
Ω_m	0.3125 ± 0.0075	0.3060 ± 0.0130	$0.3520^{+0.0320}_{-0.0270}$	$0.3096^{+0.0070}_{-0.0069}$	$0.3054^{+0.0089}_{-0.0090}$	$0.3094^{+0.0097}_{-0.0100}$
H_0	67.4 ± 1.2	68.1 ± 1.7	$63.6^{+2.3}_{-3.2}$	68.0 ± 1.1	68.3 ± 1.2	$67.8^{+1.3}_{-1.4}$
σ_8	0.831 ± 0.017	$0.839^{+0.022}_{-0.023}$	$0.802^{+0.025}_{-0.031}$	0.835 ± 0.017	0.841 ± 0.018	$0.839^{+0.018}_{-0.017}$
χ^2_{min}	12950.28	12950.23	12947.26	13657.29	13656.34	13655.36

Table 4. Fitting results for the Λ CDM, w CDM, and w_0w_a CDM models from the Planck+BSH+LSS data combination. Here, we fix $\sum m_\nu=0.06$ eV. We quote the $\pm 1\sigma$ errors. Note H_0 is in units of $\text{km s}^{-1}\text{Mpc}^{-1}$.

Data Model	Planck+BSH+LSS		
	Λ CDM	w CDM	w_0w_a CDM
$\Omega_b h^2$	0.02231 ± 0.00018	$0.02227^{+0.00021}_{-0.00023}$	0.02225 ± 0.00023
$\Omega_c h^2$	0.1171 ± 0.0027	$0.1170^{+0.0027}_{-0.0028}$	$0.1169^{+0.0028}_{-0.0029}$
$100\theta_{\text{MC}}$	1.04107 ± 0.00042	$1.04107^{+0.00040}_{-0.00045}$	$1.04107^{+0.00043}_{-0.00042}$
τ	0.063 ± 0.012	0.060 ± 0.014	$0.059^{+0.015}_{-0.017}$
w	...	-1.014 ± 0.042	$-0.99^{+0.09}_{-0.09}$
w_a	$-0.09^{+0.41}_{-0.32}$
N_{eff}	2.99 ± 0.16	$2.97^{+0.18}_{-0.19}$	2.95 ± 0.19
n_s	$0.9662^{+0.0067}_{-0.0069}$	$0.9644^{+0.0085}_{-0.0087}$	0.9637 ± 0.0087
$\ln(10^{10} A_s)$	3.052 ± 0.023	3.046 ± 0.029	$3.044^{+0.031}_{-0.035}$
Ω_m	$0.3055^{+0.0067}_{-0.0068}$	$0.3041^{+0.0086}_{-0.0087}$	$0.3041^{+0.0088}_{-0.0095}$
H_0	67.7 ± 1.1	67.9 ± 1.2	67.8 ± 1.2
σ_8	0.807 ± 0.011	0.808 ± 0.012	0.809 ± 0.012
χ^2_{min}	13903.20	13902.14	13901.12

ACKNOWLEDGEMENTS

This work is supported by the Top-Notch Young Talents Program of China, the National Natural Science Foundation of China (Grant No. 11522540), and the Fundamental Research Funds for the Central Universities (Grant No. N140505002).

REFERENCES

- Abazajian K. N., et al., 2014, *A&A*, 63, 66
 Abbiendi A., et al., 2001, *EPJC*, 19, 587
 Ade P. A. R., et al., 2013, *A&A*, 571, A16
 Ade P. A. R., et al., 2015, *arXiv:1502.01589*
 Ade P. A. R., et al., 2015, *arXiv:1502.01590*
 Ade P. A. R., et al., 2015, *arXiv:1502.01591*
 Ade P. A. R., et al., 2015, *arXiv:1502.01597*
 Aghanim N., et al., *arXiv:1507.02704*
 Aliani P., Antonelli V., Picatiello M., Torrente-Lujan E., 2003, *hep-ph/0309156*
 Anderson L., Aubourg E., Bailey S., et al., 2014, *MNRAS*, 441, 24
 Archidiacono M., Giusarma E., Hannestad E., Mena O., 2013, *Phys.Rev.D*, 87, 103519
 , Bashinsky S., Seljak U., 2004, *Phys.Rev.D*, 69, 083002
 , Battye R. A., Moss A., 2014, *Phys.Rev.Lett*, 112, 051303
 Betoule M., Kessler R., Guy J., 2014, *A&A*, 568, A22
 Beutler F., Blake C., Colless M., et al., 2011, *MNRAS*, 416, 3017
 Bond J. R., Efstathiou G., Silk J., 1980, *Phys.Rev.Lett*, 45, 1980
 Chevallier M., Polarski D., 2001, *International Journal of Modern Physics D*, 10, 2013
 Di Valentino E., Gariazzo S., Giusarma E., Lattanzi M., Mena O., 2015, *Phys.Rev.D*, 91, 123505
 Di Valentino E., Giusarma E., Lattanzi M., Mena O., Melchiorri A., Silk J., 2016, *Phys.Lett.B*, 752, 182
 Dunkley J., Hlozek R., Sievers J., et al., 2011, *ApJ*, 739, 52
 Efstathiou G., 2014, *MNRAS*, 440, 1138
 Erben T., Hildebrandt H., Miller L., 2013, et al., *MNRAS*, 433, 2545
 Hannestad S., 2005, *Phys.Rev.Lett*, 95, 221301
 Hannestad S., 2010, *Prog. Part. Nucl. Phys.*, 07, 001
 Hall A. C. & Challinor A., 2012, *MNRAS*, 425, 1170
 Heymans G., Van Waerbeke L., Miller L., et al., 2012, *MNRAS*, 427, 146
 Hinshaw G., Larson D., Komatsu E., Spergel, D. N., 2013, *Astrophys. J. Suppl*, 208, 19
 Hou Z., Reichardt C. L., Story K. T., et al., 2014, *ApJ*, 782, 74
 Howlett C., Lewis A., Hall A., 2012, *JCAP*, 1204, 027
 Hu W., Dodelson S., 2002, *ARA&A*, 40, 171
 Huang Q. G., Wang K., Wang S., 2015, *arxiv:1512.05899*
 Ichikawa K., Fukugita M., Kawasaki M., 2005, *Phys.Rev.D*, 71, 043001
 Kaplinghat M., Knox L., Song Y.-S., 2003, *Phys.Rev.Lett*, 91, 241301
 KATRIN collaboration, 2001, *arXiv:hep-ex/0109033*
 Keisler R., Reichardt C. L., Aird K. A., et al., 2011, *ApJ*, 743, 28
 Klapdor-Kleingrothaus H. V., Dietz A., Harney H., 2001, *Mod. Phys. Lett.*, 16, 2409
 Klapdor-Kleingrothaus H. V., Krivosheina I. V., Dietz A., 2004, *Mod. Phys.Lett.B*, 586, 198
 Komatsu E., Smith K. M., Dunkley J., et al., 2011, *ApJS*, 192, 18
 Kraus C., et al., 2005, *EPJC*, 40, 447
 Legourgues J., Pastor S., 2006, *Phys. Repts.*, 429, 307
 Legourgues J., Pastor S., 2012, *Adv. High Energy Phys*, 608515
 Lewis A., Bridle S., 2002, *Phys.Rev.D*, 66, 103511
 Li Y. H., Zhang X., 2012, *Phys.Lett.B*, 713, 160
 Li M., Li X. D., Ma Y. Z., Zhang X., Zhang Z., 2013, *JCAP*, 1309, 021
 Li Y. H., Wang S., Li X. D., Zhang X., 2013, *JCAP*, 1302, 033
 Li Y. H., Zhang X., 2013, *Phys.Rev.D*, 89, 083009
 Linder E. V., 2006, *Astroparticle Physics*, 26, 102
 Linder E. V., 2008, *General Relativity and Gravitation*, 40, 329
 Mangano G., Miele G., Pastor S., Pinto T., Pisanti O., & Serpico P. D., 2005, *MNRAS*, 446, 2205
 Olive K. A., 2014, *Chin. Phys.*, 38, 090001
 Otten E. M., Weinheimer C., 2008, *Reports on Progress in Physics*, 71, 086201
 Riess A. G., et al., 2011, *AJ*, 730, 119
 Robertson R. G. H., 2013, *arxiv:1307.5486*
 Ross A. J., Samushia L., Howlett, C., et al., 2014, *arXiv:1409.3242*
 Samushia L., Reid B. A., White M., et al., 2014, *MNRAS*, 439, 3504
 Smith A., Archidiacono M., Cooray A., Bernardis F. D., Mel-

- chiorri A., Smidt J., 2011, *Phys.Rev.D*, 85, 123521
- Valle J. W. F., 2006, *AIP Conf. Pro.*, 805, 128
- Wang S., Wang, Y. F., Xia D. M., 2016, Zhang X.,
arxiv:1608.00672
- Wolf J., KATRIN Collaboration, 2010, *Nuclear Instruments and
Methods in Physics Research A*, 623, 442
- Wyman M., Rudd D. H., Vanderveld R. A., Hu W., 2014,
Phys.Rev.Lett, 112, 051302
- Zablocki A., 2014, arXiv:1411.7387
- Zaldarriaga M., Harari D. D., 1995, *Phys.Rev.D*, 52, 3276
- Zhang J. F., Li Y. H., Zhang X., 2014, *EPJC*, 74, 2754
- Zhang J. F., Geng J. J., Zhang X., 2014, *JCAP*, 1410, 044
- Zhang J. F., Zhao M. M., Li Y. H., Zhang X., 2015, *JCAP*, 1504,
038
- Zhang X., 2016, *Phys.Rev.D*, 93, 083011.